Effect of inner-surface roughness of conical target on laser absorption and fast electron generation*

Wang Huan(王 欢)[a)b)], Cao Li-Hua(曹莉华)[a)b)c)†], Zhao Zong-Qing(赵宗清)[d)], Yu Ming-Yang(郁明阳)[e)f)], Gu Yu-Qiu(谷渝秋)[d)], and He Xian-Tu(贺贤土)[a)b)c)e)‡]

[a)] *Center for Applied Physics and Technology, Peking University, Beijing* 100871, *China*
[b)] *Key Laboratory of High Energy Density Physics Simulation of the Ministry of Education, Peking University, Beijing* 100871, *China*
[c)] *Institute of Applied Physics and Computational Mathematics, Beijing* 100088, *China*
[d)] *Laser Fusion Research Center, China Academy of Engineering Physics, Mianyang* 621900, *China*
[e)] *Institute for Fusion Theory and Simulation, Zhejiang University, Hangzhou* 310027, *China*
[f)] *Institute for Theoretical Physics I, Ruhr University, Bochum D*-44780, *Germany*

(Received 21 October 2013; revised manuscript received 26 December 2013; published online 1 April 2014)

The effect of inner-surface roughness of conical targets on the generation of fast electrons in the laser–cone interaction is investigated using particle-in-cell simulation. It is found that the surface roughness can reduce the fast-electron number (in the energy range $E > 1$ MeV) and energy, as compared to that from a cone with smooth inner wall. A scaling law for the laser reflectivity based on the vacuum-heating model is derived. Both theory and simulation indicate that laser reflection increases with the height-to-width ratio of the periodic inner surface structure and approaches that of a smooth cone as this ratio becomes zero.

Keywords: inner-surface roughness of cone target, particle-in-cell simulation, vacuum-heating model, laser reflection

PACS: 52.57.–z, 52.38.–r, 52.65.Rr, 41.75.–i **DOI:** 10.1088/1674-1056/23/5/055202

1. Introduction

In the fast ignition (FI) scheme of inertial confinement fusion, the laser-precompressed dense fuel core is locally ignited by energetic electrons produced from the interaction of a laser drive (hundreds of kJ in energy and 10 ps in pulse length) with a solid target or the outer part of the fuel plasma.[1] One of the challenges is how to effectively guide or transport the energetic electrons generated in the relativistic critical density region to a suitable ignition point in the ultra-dense compressed plasma over hundreds of micrometers. A practical scheme is to impinge a laser driving pulse on a cone inserted into the fuel pellet, since the cone can shield the ignition laser pulse from the corona plasma as well as guide the generated energetic electrons to the cone tip, which is deeply inside the high-density region of the pre-compressed fuel.[2–6] Accordingly, the efficiency of fast-electron generation and propagation in the cone are the key issues of this scheme. To improve the laser-to-electron energy conversion efficiency and the energetic-electron propagation properties, targets with different surfaces have been proposed and investigated extensively both experimentally and numerically.[7–17]

Many novel tailored cone targets designed to improve the electron generation and transport have been proposed.[2,18–21] Particularly, the structured surface with sub-wavelength periodic patterns can greatly enhance laser absorption or fast electron number.[7,13,22,23]

In practice, the inner wall of the conical target is not smooth. The effect of inner surface roughness on laser absorption, as well as on the generation and propagation of fast electrons, has not been investigated in detail. In this paper, we model the roughness of the inner cone wall by assuming a periodic corrugated surface, and consider the interaction between the laser light with the latter structure. To investigate the effect of the surface roughness on laser absorption and fast-electron generation and transport, we carry out two-dimension-in-space and three-dimension-in-velocity (2D3V) particle-in-cell (PIC) simulations on the interaction process, as well as obtain analytically a scaling law for the laser reflectivity based on the vacuum-heating model.

In Section 2, we present the target model and the simulation parameters. For comparison, both smooth and corrugated conical targets shall be considered. In Section 3, the effect of inner surface roughness on laser reflection is examined analytically and numerically. In Section 4, the effect of roughness on the properties of the generated fast electrons is considered. A summary is given in Section 5.

*Project supported by the National Natural Science Foundation of China (Grant Nos. 11175030, 11175029, 91230205, and 11375032), the National High-Tech ICF Committee of China, the National Basic Research Program of China (Grant Nos. 2008CB717806 and 2011CB808104), and the Science and Technology Foundation of China Academy of Engineering Physics (Grant No. 2011A0102008).

†Corresponding author. E-mail: cao_lihua@iapcm.ac.cn
‡Corresponding author. E-mail: xthe@iapcm.ac.cn

© 2014 Chinese Physical Society and IOP Publishing Ltd

2. Target configuration and simulation parameters

A 2D3V PIC code is used to simulate the response of a conical target with corrugated inner surface to a p-polarized intense laser pulse.[24] Figure 1(a) schematically shows a cone target with smooth inner surface and figure 1(b) a target with rough inner surface. For simplicity, the latter is assumed to have a sinusoidal structure given by $y(z) = z\tan\theta_0 + \frac{h}{2} - \frac{h}{2}\sin\left(\frac{2\pi z}{d}\right)$, where d and h are the actual width and height of the sinusoidal structure, respectively. The cone has a full-opening angle of 34°, with 4λ thick wall and an inner tip width of 8λ, where $\lambda = 1$ μm is the vacuum laser wavelength. Both targets are assumed to be pre-ionized Cu^{5+} plasma with initial electron density $n_0 = 10n_c$, where n_c is the critical density. The initial temperatures of the electrons and ions are 100 eV.

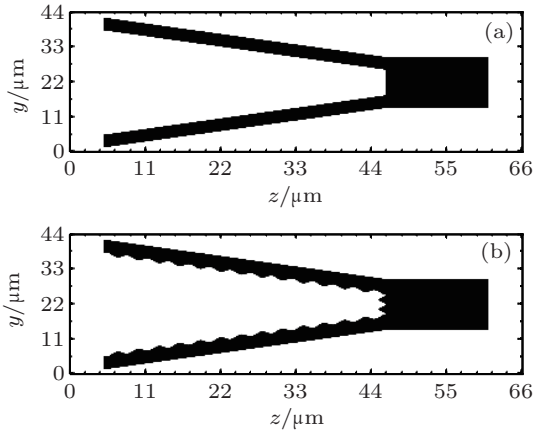


Fig. 1. (a) Cone target with smooth inner surface, and (b) cone target with corrugated inner surface. The cone has a 34° full-opening angle with 4λ thick wall and an internal tip width of 8λ.

The size of the simulation box is 44×66 μm^2. The laser propagates along the z axis and (y, z) is the simulation plane. A p-polarized laser pulse is incident normally from the left boundary of the simulation box. The laser pulse rises exponentially for $8T$, where T is the laser cycle and remains at the peak intensity for $102T$. The laser parameter is $a_0 = eE_0/m\omega_0 c \sim 6.4$, which corresponds to the laser intensity $I \approx 5.6 \times 10^{19}$ W/cm^2, where $-e$, m, ω_0, E_0, and c are the electron charge, electron rest mass, laser-light frequency, maximum laser electric field amplitude, and speed of light in vacuum, respectively. The laser axis is at $y = y_0 = 22\lambda$ and the transverse profile of laser pulse is Gaussian with spot radius $w = 10\lambda$. Unless otherwise stated, the simulations are performed with these parameters.

The laser prepulse effect is precluded in our simulation assuming that the laser pulse has a contrast ratio larger than 10^9.

3. Effect of surface roughness on laser absorption

An analytic expression for the laser reflectivity is obtained using the vacuum-heating model.[25,26] We assume that the electrons at the sharp edge of the plasma-vacuum interface are directly exposed to the laser field. A thermal electron arriving near the plasma–vacuum interface at the right phase of the laser cycle is dragged out into the vacuum beyond a Debye sheath $\lambda_D = v_{te}/\omega_p$, where v_{te} is the thermal velocity of the electron and ω_p is the electron plasma frequency. As the field reverses its direction, the electron is accelerated back into the plasma. The laser electric field E_L has a component $E_d = E_L \sin\theta_0$ normal to the cone surface, and it drives the electrons back and forth. The laser acting on the smooth cone wall with an incident angle $\theta_0 = 73°$ is split into two equal components at equal and opposite angles of incidence due to light reflection and a standing wave will be set up. The driving electric field normal to the surface becomes $E_d = 2E_L \sin\theta_0$ and the maximum electric field positions correspond to magnetic field nodes, so that the magnetic Lorentz force can be neglected.[25] Suppose this field pulls a sheet of electrons out to a distance of Δx from its initial position, a charge-separation electrostatic field $\Delta E = 4\pi e\sigma$, where σ is the surface number density of the sheet and given by $\sigma = 2E_L \sin\theta_0/4\pi e$, will be created. When the electron sheet returns to its original position, it will acquire a driven velocity of $v_d \simeq 2v_{osc}\sin\theta_0$, where $v_{osc} = eE_L/m_e\omega_0$. Assuming that the kinetic energies of these electrons are all from the laser irradiance, then the average energy density absorbed per laser cycle is

$$P_a = \frac{\sigma m_e}{T}\frac{v_d^2}{2} \simeq \frac{1}{16\pi^2}\frac{e}{m_e\omega_0}E_d^3.$$

Comparing it to the incoming laser power, we can obtain the laser absorption rate as

$$\eta_a = \frac{P_a}{P_L} = \frac{4a_0}{\pi}\frac{\sin^3\theta_0}{\cos\theta_0}.$$

Figure 2 plots a schematic diagram of the incident laser and the corrugated conical target. The points M and N (red dots) mark adjacent peaks on the corrugation surface, and point D (red dot) is the intersection of the corrugation surface and the line (parallel to the z axis) passing through M. The black arrow on the left indicates the direction of the incident laser, where θ is the angle between the incident laser and the normal (black dash-dot line) to the inner cone surface at the laser impact point K. The angle θ_1 is measured from the line OM to the z axis, where O is the origin (0, 0). Taking into account the reduced driver field amplitude due to imperfect reflectivity, we replace E_d by $E_d = \left(1 + \sqrt{1-\eta_a}\right)E_L \sin\theta$. It should be noted that now the incident angle θ is not constant. Instead, it depends on the location of laser field on the rippled

surface. The return velocity of the electrons becomes relativistic at intensity of 10^{19} W/cm^2. We should introduce the relativistic correction, that is, the absorbed laser energy over one laser period is denoted as $2\pi\sigma(\gamma-1)m_ec^2$ by replacing the electron kinetic energy by $(\gamma-1)m_ec^2$, where $\gamma=\sqrt{1+v_d^2/c^2}$ and $v_d/c \simeq \left(1+\sqrt{1-\eta_a}\right)a_0\sin\theta$. Using the above corrections, an implicit expression is arrived

$$R(\theta)=1-\frac{1}{\pi a_0}f\left[\left(1+f^2a_0^2\sin^2\theta\right)^{1/2}-1\right]\frac{\sin\theta}{\cos\theta}, \quad (1)$$

where $f=1+\sqrt{1-\eta_a}$.

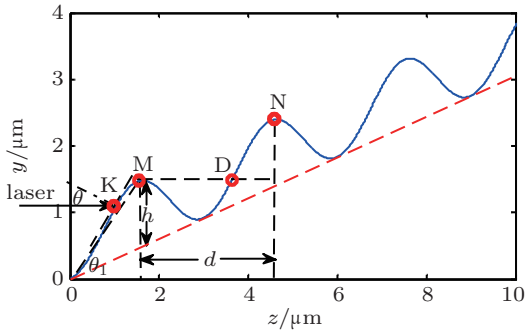


Fig. 2. (color online) Schematic diagram showing the incident laser and the corrugated conical target surface. The points M and N are adjacent peaks on the corrugated surface, and the point D is the intersection of the corrugation surface and the line parallel to the z axis and passing through M. The black arrow on the left marks the incident laser, where θ is the angle between the incident laser and the local normal (black dash-dotted line) to the corrugation surface at the laser impact point K. The angle θ_1 is the angle between the line OM and the z axis, where O is the origin $(0, 0)$. Furthermore, the corrugation period d is the distance between M and N, and the corrugation height h is the distance between M and the base (red dashed line) of the corrugation.

The above expression can be simplified in the relativistic limit ($a_0 > 1$). In the condition considered here, $fa_0\sin\theta > 1$, we can get $\eta_a = f^2\sin^2\theta/(\pi\cos\theta)$. Finally, the laser reflectivity can be achieved by letting $\alpha=\sin^2\theta/\cos\theta$, that is,

$$R(\theta)=1-\frac{4\pi\alpha}{(\pi+\alpha)^2}. \quad (2)$$

From M to N, the reflectivity in one period of the corrugated surface is

$$R=\frac{\psi}{z_N-z_D}\int_{z_D}^{z_N}R(z)\,dz, \quad (3)$$

where ψ is a shape factor and depends on the laser transverse shape. It is assigned as $\psi=0.586$ with the Gaussian laser profile of $\exp\left[-(y-22)^2/10^2\right]$. The angle between the line OM and the z axis is $\tan\theta_1=\tan(90^\circ-\theta_0)+2\kappa$, where $\theta_0=73^\circ$ and $\kappa=h/d$ is the height-to-width ratio, or the corrugation parameter, of the surface corrugation. Accordingly, the reflectivity R can be written as

$$\frac{R}{\psi}=1-\frac{1}{\zeta}\log\left(1+\frac{4\zeta}{\chi}\right)+\frac{4}{\chi(\chi+4\zeta)}, \quad (4)$$

where $\zeta=\pi\kappa/\sin\theta_1$, and $\chi=1+1/\cos\theta_1$.

The solid curve in Fig. 3 shows the dependence of the reflectivity on the corrugation parameter κ from the analytical expression (3). The result from PIC simulations (averaged from $10T$ to $90T$) are given by the cyan square, red circles, blue diamonds, green plus, and magenta cross for $\kappa=0$, 1/6, 1/4, 1/3, 1/2, 1, 3/2, and 2, where the cyan square, blue diamonds, red circles, green plus, and magenta cross are for $h=0\lambda$, 0.5λ, 1λ, 1.5λ, 2λ, respectively. As shown in Fig. 3, the analytic scaling law for the dependence of the laser reflectivity on the corrugation parameter κ obtained from the vacuum-heating model fits approximately with the simulation results for different κ values of the periodic corrugation structure. Figure 3 also shows that the reflectivity increases with κ as expected since the reflection surface becomes larger. For the same corrugation parameters ($\kappa=1/3$ and $\kappa=1/2$) but different values of h, the red circles and blue diamonds are for $h=1\lambda$ and $h=0.5\lambda$, respectively. We see that the surface with lager h leads to larger reflectivity even if κ remains the same. That is, the laser reflectivity is more sensitive to height h of the corrugation than the width d. Furthermore, for $h\to 0$ or $d\to\infty$, the reflectivity approaches that (cyan square in Fig. 3) obtained from the analytical expression (3) for a smooth inner-surface cone.

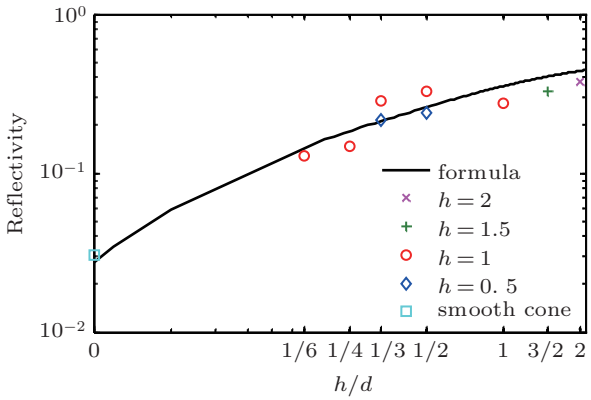


Fig. 3. (color online) Dependence of the laser reflectivity on $\kappa=h/d$. The solid curve is from the theoretical scaling law given by the formula (3), and the cyan square, red circles, blue diamonds, green plus, and magenta cross are from the simulations (averaged from $10T$ to $90T$) for $\kappa=0$, 1/6, 1/4, 1/3, 1/2, 1, 3/2, and 2, where the cyan square, blue diamonds, red circles, green plus, and magenta cross are for $h=0$, 0.5λ, 1λ, 1.5λ, 2λ, respectively. The corresponding h values (in units of λ) are given in the legend.

4. Role of inner surface roughness in generation of fast electrons

We now investigate the influence of the surface roughness of the conical target on the characteristics of the fast electrons generated by the laser–plasma interaction. It is a basis in the applications such as FI,[1] novel high-brightness X-ray, and K_α sources.[27]

Figure 4 shows the energy spectrum of fast electrons in the cone tip region (45 μm $< z <$ 55 μm and 15.8 μm $< y <$

24.2 μm) at 110T for both smooth surface (black solid line) and corrugated surface (red dashed line), and we can see that energy spectrum of fast electrons generated by the corrugated target is softer than that by the ideal cone target. According to our vacuum heating model in Section 3, the laser reflectivities for corrugated cone targets are larger than the smooth cone, namely, the laser irradiation energy absorbed by the fast electrons produced in corrugated cone is lower than that in a smooth cone. When these fast electrons propagate along the cone walls towards the cone tip region (45 μm $< z <$ 55 μm and 15.8 μm $< y <$ 24.2 μm), smooth cone walls have no impediment to go forward, while rough cone walls prohibit them from approaching the cone tip smoothly. Therefore, spectrum of fast electron generated by the corrugated cone target is softer due to the higher laser reflection as a result of the rough inner surface.

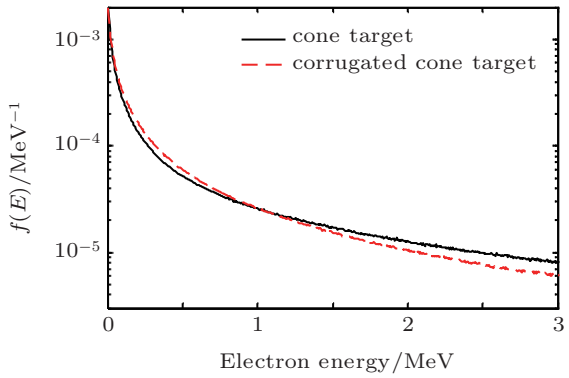


Fig. 4. (color online) Energy spectrum of the fast electrons (1 MeV $<$ $E <$ 2 MeV) in the cone tip region (45 μm $< z <$ 55 μm and 15.8 μm $<$ $y <$ 24.2 μm) at 110T for the smooth cone (black solid curve) and the corrugated cone (red dashed curve).

Figure 5 shows time evolution of number of fast electrons with kinetic energies $E >$ 1 MeV in the cone tip region (45 μm $< z <$ 55 μm and 15.8 μm $< y <$ 24.2 μm) during 110T for the smooth cone (black solid line) and corrugated cone (red dashed line). At the beginning ($t \leq 64T$), the corrugation on the inner wall leads to more energetic electron production since the interaction area and the range of incidence angles are significantly larger in the laser–target interaction. However, at later times there is less laser-energy absorption due to laser reflection from the enhanced preplasma, and the forward motion of the electrons is also hindered by the induced electric and magnetic fields. As a result, the number of fast electrons generated from a corrugated surface becomes less than that from a smooth surface.

The five-laser-cycle averaged longitudinal current J_z at $t =$ 110T is shown in Figs. 6(a) and 6(b). Because of the periodic inner cone surface, J_z is no longer continuous and monotonic, like that for the smooth cone. Although the current is still along the corrugation surface, but it appears to be discontinuous. The negative currents ($J_z < 0$) at the crests of the rippled structure originate from the forward-propagating fast electrons. The positive currents closer to the surface of the rippled structure are associated with the returned-current electrons propagating backwards. The current induces electric and magnetic fields. Our simulation results yield $J_z \sim 6.6 \times 10^{17}$ A/m^2 for the smooth and $J_z \sim 6.0 \times 10^{17}$ A/m^2 for the corrugated cone surfaces. This drop can be attributed to less laser absorption due to increased reflection and hindrance of the forward electron motion by the large-amplitude ripples in the induced electric and magnetic fields.

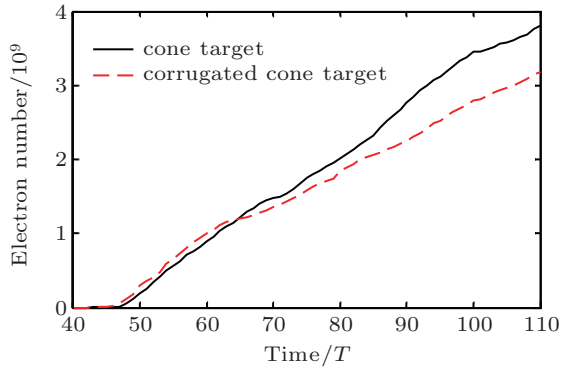


Fig. 5. (color online) Time evolution of number of fast electrons with kinetic energy $E >$ 1 MeV in the cone tip region (45 μm $< z <$ 55 μm and 15.8 μm $< y <$ 24.2 μm) at 110T for the smooth (black solid curve) and the corrugated (red dashed curve) cone.

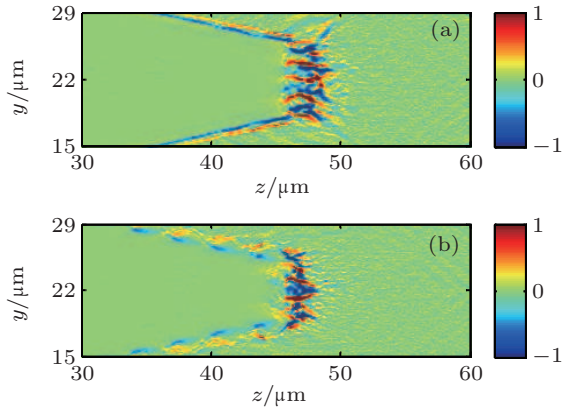


Fig. 6. (color online) Snap shots of longitudinal current component J_z for (a) the smooth conical target and (b) the corrugated conical target, both at time 110T. The longitudinal current component J_z is averaged over five laser cycles and normalized by n_0ec.

For comparison, the average induced electric and magnetic fields at 110T for the smooth and corrugated cone surfaces are presented in Figs. 7(a)–7(d), respectively. Significantly different electric field configurations can be observed. For the corrugated cone surface, as shown in Fig. 7(c), the induced electric field has a regular periodic structure. The positive electric fields tend to drive the electrons backward, and the negative fields tend to drive the electrons forward. In fact, some electrons are trapped in the periodic structure, and cannot propagate forward to the cone tip. Figure 7(d) shows

that around the corrugated inner cone surface the induced magnetic field B_x is in the form of a string of localized clumps, or magnetic islands, with a spatial scale of 3λ, which is roughly the same as the period d of the surface structure. This magnetic field configuration can be attributed to the two corrugated sheets of longitudinal current J_z, as shown in Fig. 6(b). The sheet currents are in opposite directions, with the negative J_z having substantially larger magnitude. As a result, the discontinuous but unidirectional B_x in the corrugation valleys can drive the fast electrons forward. From the Ampere's law and the value of J_z found in Fig. 6, the magnitude of the magnetic field can be estimated to be $B_x \approx 3 \times 10^8$ Gs, which agrees fairly well with the simulation result shown in Fig. 7(d).

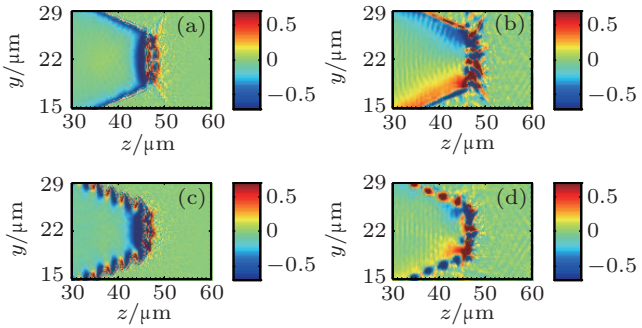


Fig. 7. (color online) Snap shots of the fields at $t = 110T$. (a) Longitudinal electric field E_z and (b) magnetic field B_x for the smooth-surface cone. (c) Longitudinal electric field E_z and (d) magnetic field B_x for the corrugated-surface cone. The magnetic and electric fields are averaged over five laser cycles and in units of 3×10^{10} V/cm and 10^8 Gs, respectively.

5. Summary

In summary, the effect of inner-surface roughness of conical targets on laser absorption and generation of fast electrons in the FI scheme of ICF is investigated using 2D3V PIC simulations and theoretical modeling. It is shown that a corrugated conical target with periodic inner-wall surface structure leads to higher laser reflection and slightly less efficient generation of fast electrons in that the energy spectrum is softer and the number is less. A scaling law for the laser reflectivity is derived using the vacuum-heating model. The theory as well as the simulation show that laser reflection increases with the height-to-width parameter κ of the periodic corrugation and approaches that of the smooth surface in the limit $\kappa \to 0$. With the corrugated surface, the laser generated fast electrons in the skin layer of the inner wall are trapped and slowed by the induced electric and magnetic fields. Our results indicate that the smoothness of the inner surface should be taken into consideration in the fabrication of cone targets for ICF.

References

[1] Tabak M, Hammer J, Glinsky M E, Kruer W L, Wilks S C, Woodworth J, Campbell E M, Perry M D and Mason R J 1994 *Phys. Plasmas* **1** 1626

[2] Kodama R, Norreys P A, Mima K, Dangor A E, Evans R G, Fujita H, Kitagawa Y, Krushelnick K, Miyakoshi T, Miyanaga N, Norimatsu T, Rose S J, Shozaki T, Shigemori K, Sunahara A, Tampo M, Tanaka K A, Toyama Y, Yamanaka Y and Zepf M 2001 *Nature* **412** 798

[3] Cai H B, Mima K, Zhou W M, Jozaki T, Nagatomo H, Sunahara A and Mason R J 2009 *Phys. Rev. Lett.* **102** 245001

[4] Sentoku Y, Mima K, Ruhl H, Toyama Y, Kodama R and Cowan T E 2004 *Phys. Plasmas* **11** 3083

[5] Nakamura T, Sakagami H, Hohzaki T, Sakagami H, Johzaki T, Nagatomo H, Mima K and Koga J 2007 *Phys. Plasmas* **14** 103105

[6] Liu H J, Gu Y Q, Zhou W M, Yu J Q, Zhu B, Wu Y C, Shan L Q, Wen X L, Li F, Qian F, Cao L F, Zhang B H and Zheng Z J 2012 *Chin. Phys. B* **21** 055207

[7] Kahaly S, Yadav S K, Wang W M, Sengupta S, Sheng Z M, Das A, Kaw P K and Kumar G R 2008 *Phys. Rev. Lett.* **101** 145001

[8] Cao L H, Yu W, Yu M Y, Xu H, He X T, Gu Y Q, Liu Z J, Li J H and Zheng C Y 2008 *Phys. Rev. E* **78** 036405

[9] Liu Z J, Zheng C Y, Cao L H, Li B and Zhun S P 2006 *Acta Phys. Sin.* **55** 304 (in Chinese)

[10] Kulcsár G, Mawlawi D Al, Budnik F W, Herman P R, Moskovits M, Zhao L and Marjoribanks R S 2000 *Phys. Rev. Lett.* **84** 5149

[11] Lei A L, Tanaka K A, Kodama R, Kumar G R, Nagai K, Norimatsu T, Yabuuchi T and Mima K 2006 *Phys. Rev. Lett.* **96** 255006

[12] Murnane M M, Kapteyn H C, Gordon S P, Bokor J, Glytsis E N and Falcone R W 1993 *Appl. Phys. Lett.* **62** 1068

[13] Cao L H, Gu Y Q, Zhao Z Q, Cao L F, Huang W Z, Zhou W M, He X T, Yu Wei and Yu M Y 2010 *Phys. Plasmas* **17** 043103

[14] Cao L, Chen M, Zhao Z, Cai H, Wu S, Gu Y, Yu W, Yu M Y and He X T 2011 *Phys. Plasmas* **18** 054501

[15] VanWoerkom L, Akli K U, Bartal T, Beg F N, Chawla S, Chen C D, Chowdhury E, Freeman R R, Hey D, Key M H, King J A, Link A, Ma T, MacKinnon A J, MacPhee A G, Offermann D, Ovchinnikov V, Patel P K, Schumacher D W, Stephens R B and Tsui Y Y 2008 *Phys. Plasmas* **15** 056304

[16] Micheau S, Debayle A, d'Humières E, Honrubia J J, Qiao B, Zepf M, Borghesi M and Geissler M 2010 *Phys. Plasmas* **17** 122703

[17] Chrisman B, Sentoku Y and Kemp A J 2008 *Phys. Plasmas* **15** 056309

[18] Zhou C T, He X T and Yu M Y 2008 *Appl. Phys. Lett.* **92** 151502

[19] Winterberg F 2004 *Phys. Plasmas* **11** 3955

[20] King J A, Akli K U, Freeman R R, Green J, Hatchett S P, Hey D, Jamangi P, Key M H, Koch J, Lancaster K L, Ma T, MacKinnon A J, MacPhee A, Norreys P A, Patel P K, Phillips T, Stephens R B, Theobald W, Town R P J, Van Woerkom L, Zhang B and Beg F N 2009 *Phys. Plasmas* **16** 020701

[21] Liu F, Lin X X, Liu B C, Ding W J, Du F, Li Y T, Ma J L, Liu X L, Sheng Z M, Chen L M, Lu X, Dong Q L, Wang W M, Wang Z H, Wei Z Y and Zhang J 2012 *Phys. Plasmas* **19** 013103

[22] Wang W M, Sheng Z M and Zhang J 2008 *Phys. Plasmas* **15** 030702

[23] Hu G Y, Lei A L, Wang J W, Huang L G, Wang W T, Wang X, Xu Y, Shen B F, Liu J S, Yu W, Li R X and Xu Z Z 2010 *Phys. Plasmas* **17** 083102

[24] Ruhl H, Bonitz M and Semkat D 2006 *Introduction to Computational Methods in Many Particle Body Physics* (New Jersey: Rinton Press)

[25] Brunel F 1987 *Phys. Rev. Lett.* **59** 52

[26] Gibbon P 2005 *Short Pulse Laser Interactions with Matter* (London: Imperial College Press) pp. 158–161

[27] Rousse A, Rischel C and Gauthier J C 2001 *Rev. Mod. Phys.* **73** 17

[28] Murnane M M, Kapteyn C, Rosen M and Falcone R W 1991 *Science* **251** 531

[29] Kieffer J C, Chaker M, Matte J P, Pépin H, Côté C Y, Beaudoin Y, Johnston T W, Chien C Y, Coe S, Mourou G and Peyrusse O 1993 *Phys. Fluids B* **5** 2676